

A multi-sensor and modeling analysis of a severe convective storm in Lake Maggiore area (northwestern Italy)

Avolio E. ^{1,*}, Nisi L. ², Panziera L. ², Peyraud L. ³ and Miglietta M.M. ⁴

1- Institute of Atmospheric Sciences and Climate – National Research Council (ISAC-CNR), Lamezia Terme, Italy

2- Federal Office of Climatology and Meteorology, MeteoSwiss, Locarno-Monti, Switzerland

3- Federal Office of Climatology and Meteorology, MeteoSwiss, Geneva, Switzerland

4- Institute of Atmospheric Sciences and Climate – National Research Council (ISAC-CNR), Padua, Italy

* corresponding author: Elenio Avolio, ISAC-CNR, c/o Area Industriale, compartment 15, I-88046 Lamezia Terme, Italy. (E-mail address: e.avolio@isac.cnr.it).

Abstract

The analysis of a severe convective storm occurred in northwestern Italy during late summer 2012 is presented here. The event was characterized by heavy precipitation, hail and intense wind gusts, causing injuries and damages to trees, buildings and infrastructures.

The description of the case study draws upon a wide palette of observational data. Surface and upper-air observations helped characterize the event, emphasizing the rapid changes in the meteorological parameters in the study area; satellite data highlights the presence of deep moist convection, associated with strong updrafts; Doppler radar allows the identification of the main features of the event in terms of storm-motion, hail detection/probability and the possible presence of a mesocyclone.

A high-resolution (3 km inner grid spacing) simulation with the WRF (Weather Research and Forecasting) model was performed to study the atmospheric conditions conducive to convection, as well as to estimate the main instability parameters. The main features of the storm were well reproduced with WRF; furthermore, the high values of the simulated instability parameters denote the presence of favourable conditions for severe convection.

The analysis of this event shows that supercells can develop also in a pre-alpine environment, characterized by a complex orography, in particular in the sub-regions where the local morphology creates conditions favourable for severe weather development.

Keywords: severe storm; supercell; mesocyclone; WRF; deep convection; Lake Maggiore.

1. Introduction

The Mediterranean basin is particularly prone to heavy rainfall and convective events, mainly due to the peculiar climatic characteristics of the region and to its complex morphology. Synoptic-scale patterns, Mediterranean cyclones or mesoscale convective systems (MCSs) may interact with local geographical and topographical features to develop severe weather, such as wind gusts, hail and tornadoes (Jirak et al., 2003; Schenkman et al., 2011, Jansa et al., 2014).

The inhomogeneous environment of the Mediterranean basin requires high-resolution analysis in order to take into account properly the interaction with the orography, the land–sea contrast, and the intense air–

60
61 45 sea interaction (Lionello et al. 2006). These effects determine significant small-scale variations of the
62
63 46 instability parameters, a peculiar feature compared to environments with a more homogeneous
64
65 47 morphology, e.g. the U.S. Great Plains, where the typical horizontal scale of variation is generally much
66
67 48 wider (Doswell et al. 2012). Indeed, small-scale terrain features may be crucial in forcing local circulations,
68
69 49 which, in combination with the presence of moist and warm air in the low levels, support the development
70
71 50 of severe convection (Homar et al. 2003) and supercells (Scheffknecht et al., 2017; Miglietta et al., 2016,
72
73 51 2017a, 2017b; Peyraud, 2013).

74
75 52 The Italian peninsula is occasionally affected by localized severe convective events associated with intense
76
77 53 winds, such as tornadoes and downbursts. Historical documents and press news reveal that their
78
79 54 occurrence is not rare, especially in specific sub-areas (e.g., Gianfreda et al., 2005). Such events are
80
81 55 reported only rarely in official bulletins, since synoptic stations are too sparse to provide a detailed
82
83 56 coverage of small-scale phenomena; thus, their occurrence is generally attested by amateurs' reports and
84
85 57 dedicated forum websites. Several web portals/platforms that web surfers use to share and upload pictures
86
87 58 and videos gather additional information even on weak events, which otherwise could not be reported. In
88
89 59 the absence of photographs or videos to document their occurrence, as for night-time events, the damage
90
91 60 survey is the best method to discriminate between a tornado and a straight-line wind event (e.g., a
92
93 61 microburst).

94
95 62 Using such unofficial data sources, a 10-year "climatology" of tornadoes and waterspouts in Italy was
96
97 63 undertaken a few years ago (Giaiotti et al., 2007). The Po Valley, especially its eastern side, stood out as
98
99 64 one of the Italian areas most affected by such events, primarily due to the contrast between the low-level
100
101 65 relatively warm and moist air moving northward from the Adriatic Sea and the cold upper level air
102
103 66 intrusions crossing the Alps. An updated climatology of tornadoes and waterspouts in Italy was recently
104
105 67 provided (Miglietta and Matsangouras, 2018), including a classification of these events in terms of
106
107 68 geographical, seasonal, monthly, diurnal, and rating distribution, for the period 2007–2016. The authors
108
109 69 confirmed that these events are more frequent in late spring/summer in northern Italy, occurring mainly in
110
111 70 flat areas or close to the coastlines. On average, the yearly density of tornadoes in Italy is comparable with
112
113 71 that of other Mediterranean countries (Matsangouras et al., 2014, 2017; Rodríguez and Bech, 2018), but
114
115 72 the frequency of occurrence may be much higher in specific sub-areas. Although statistics on downbursts in
116
117 73 Italy are not available, the analysis of the ESWD (European Severe Weather Database; Dotzek et al. 2009)
118
119 74 suggests that also "linear" storms (e. g., squall line) occur more frequently in summer in the Po Valley.

120
121 75 An intense event occurred in the pre-Alpine region during the evening of 25 August 2012, when a severe
122
123 76 convective storm hit the Lake Maggiore area (northwestern Italy; Figure 1), and in particular the town of
124
125 77 Verbania (coordinates LON: 8.55°E, LAT: 45.92°N). The region of Lake Maggiore is not only one of the two
126
127 78 regions with the largest amount of yearly precipitation in the Alps (Isotta et al. 2014), but is also particularly
128
129 79 prone to precipitation episodes with high rainfall intensity (Panziera et al., 2018). Heavy rainfall events are
130
131 80 usually triggered in the region by south-to-southeasterly mesoscale flows forced to ascend over the

119
120
121
122
123
124
125
126
127
128
129
130
131
132
133
134
135
136
137
138
139
140
141
142
143
144
145
146
147
148
149
150
151
152
153
154
155
156
157
158
159
160
161
162
163
164
165
166
167
168
169
170
171
172
173
174
175
176
177

81 mountains in the northwestern side of the lake in a conditionally unstable environment (Panziera et al.
82 2010, 2015). In the warm months, the area is also frequently affected by thunderstorms producing hail, in
83 particular in the southeastern side of the lake (Nisi et al. 2016).

84 In the early afternoon, the thunderstorm of 25 August 2012 was triggered to the west-south-west of lake
85 Maggiore, in the northern part of Novara province (Piedmont region; Figure 1b), where only minor
86 damages were reported; at around 18:00 UTC, the storm dramatically reinforced during its transit over the
87 lake, remaining severe farther northeastward, in the northern part of the province of Varese and in
88 southern Ticino, Switzerland, before weakening later in the evening. Torrential rain, with peaks of above
89 100 mm in 3 hours (mainly concentrated in a band about 5 km wide), localized hail and strong gusts were
90 reported in these areas. Several trees were uprooted, creating traffic problems and obstructing some minor
91 rivers; public lighting was damaged; widespread damages to houses and cars were reported and power
92 outages occurred. About twenty people were wounded, although not seriously.

93 As a consequence of the severe wind, the world-recognized botanic garden of Villa Taranto was destroyed,
94 being 350 secular trees uprooted, for an estimated damage of more than 11 million euros. (Figures 1e,f
95 show some photos of the damages near Villa Taranto.) The area has not been immune to similar events in
96 the past, since a severe wind gust (possibly a tornado) on 28 June 2006 uprooted some big trees in “Isola
97 Madre” in the Borromeo Gulf (<https://www.varesenews.it/2006/06/lago-maggiore-tromba-d-aria-sull-isola-madre/251863/>).



Fig. 1. a) The two domains used in the numerical simulation. b) The innermost WRF grid and the model terrain height (m), including the location of the places mentioned in the manuscript. c) A zoom in the Lake Maggiore area, including the location of the places mentioned in the manuscript. d) A further zoom in the Verbania area; the zones affected by damages are coloured in red (based on reports received by the Civil Protection offices of the Piedmont region; the map was available on: <http://www.verbaniamilleventi.org>). e) and f) Damages near Villa Taranto. (For interpretation of the references to colour in this figure legend, the reader is referred to the web version of this article)

The storm in Verbania was of smaller intensity compared to other severe localized storms that affected Italy in the last few years (Miglietta and Rotunno, 2016; Zanini et al., 2016), but its peculiarity was that it occurred in the area of Lake Maggiore, a prealpine area where rotating storms have not yet been documented in the literature so far, even though convective storms are frequent (Nisi et al., 2016). We consider this event worth of investigation also due its good radar data coverage, in particular the Monte Lema MeteoSwiss radar located on the northern side of Lake Maggiore and the radar of the Piedmont

237

238 115 region in Bric della Croce (which, with the radar of Monte Settepani, constitutes the radar Piedmont
239
240 116 mosaic), although the latter is too far south to provide very detailed information.

241 117 Therefore, the purpose of the present paper is twofold: on the one hand, we will identify the characteristics
242
243 118 of this storm, also using recently developed detection algorithms, in order to better understand the
244
245 119 characteristics of the environment where the supercell developed; on the other hand, we will explore how
246 120 far we can go in the prediction of this kind of events using limited area models. This is particularly relevant
247
248 121 in the Alpine area, where supercells have been documented in the literature only in a few cases; therefore,
249 122 we believe that our analysis, even if limited to a single case study, can provide valuable information for the
250
251 123 study and the prediction of similar events in the region.

252 124 The summary of the present paper is the following: after a synoptic analysis of the event in Section 2, some
253
254 125 surface observations and a nearby sounding are analysed in Section 3. Then, a satellite perspective of the
255 126 case study is provided in Section 4 and radar data are discussed in Section 5, in order to identify the main
256
257 127 features of the event using different data sources. In Section 6, limited area model simulations are
258 128 examined, focusing on some instability parameters in order to estimate the potential instability of the
259
260 129 surrounding environment. Conclusions are drawn in Section 7.

261 130

262 131

263 132

264 133

265 134

266 135

267 136

268 137

269 138

270 139

271 140

272 141

273 142

274 143

275 144

276 145

277 146

278 147

279 148

280 149

281 150

282 151

283 152

284 153

285 154

286 155

2. Synoptic conditions

A levelled mean sea level pressure field was present at 00:00 UTC, 26 August 2012 (Figure 2) over northern Italy. Considering the fields at 00:00 UTC, 26 August 2012, a levelled field of the mean sea level pressure was apparent over northern Italy (Figure 2). This configuration followed several days characterized by a persistent African anticyclone affecting the western Mediterranean region; such conditions favoured the accumulation of moist and warm air at low levels. Meanwhile, a frontal system affected the Alpine region, slowly moving southeastward. The front separated the colder air north of the Alps (bluish colours in Figure 3) from the warmer Mediterranean air on its southern side (reddish colours).

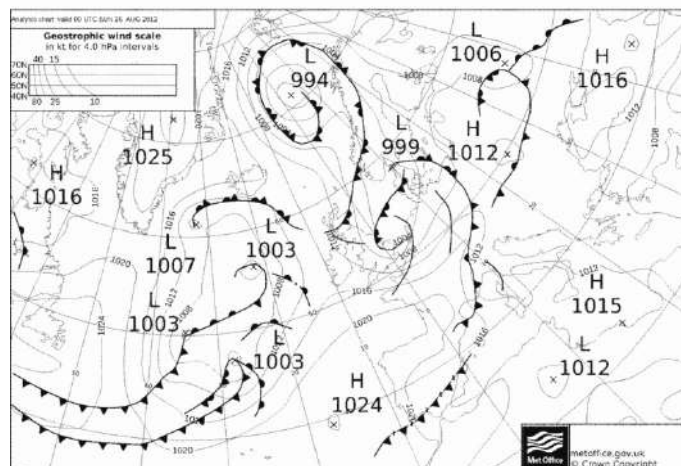


Fig. 2. Surface map (sea level pressure [hPa] and weather fronts) at 00:00 UTC, 26-08-2012 (source: metoffice.gov.uk).

296
297 143
298 144
299
300
301
302
303
304
305
306
307
308
309
310 145
311 146
312 147
313 148
314 149
315 150
316 151
317 152
318 153
319 154
320
321 155
322 156
323
324 157
325 158
326
327 159
328
329
330
331
332
333
334
335
336
337
338
339
340
341
342
343 160
344 161
345 162
346 163
347 164
348 165
349 166
350 167
351
352 168
353
354

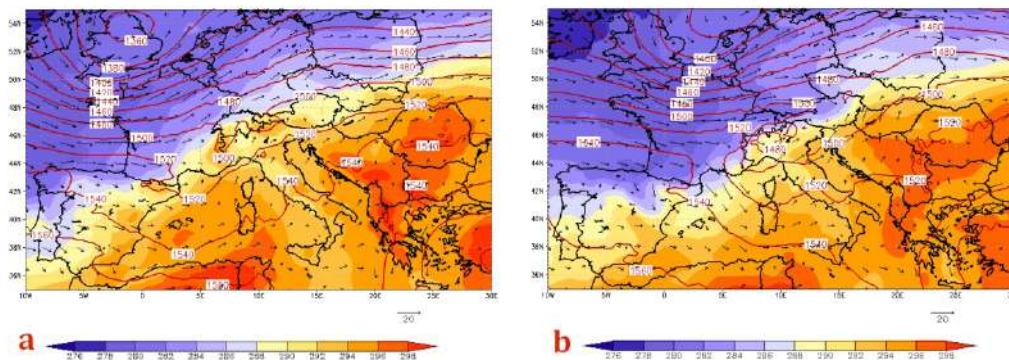


Fig. 3. 850 hPa Temperature (filled-contours, °C), geopotential height (red-contours, m) and wind vectors (m/s): 12:00 UTC, 25-08-2012 (left) and 00:00 UTC, 26-08-2012 (right). The maps are derived from **Global Forecast System (GFS)** analysis at 0.5°. (For interpretation of the references to colour in this figure legend, the reader is referred to the web version of this article)

The cooler air mass slowly penetrated from the Alpine region towards the Po valley (**Figure 1b**), producing a temperature decrease of a few K over northwestern Italy: e.g., at 850 hPa, a decrease of 4 K was observed in 12 hours (**Figure 3**), and a similar change was observed at upper levels (not shown). The combination of upper level cold air and pre-existing very hot and moist low-level air increased the potential instability of the environment. Also, the right-entrance of an upper level southwesterly jet streak (**Figure 4**), located near the Lake Maggiore area, favoured large-scale ascending motion.

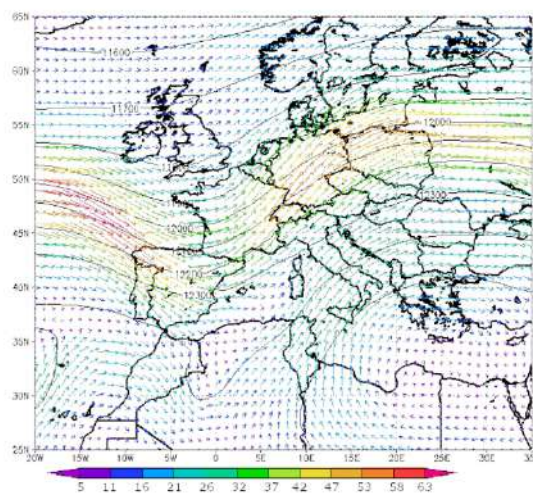


Fig. 4. 200 hPa geopotential height (black lines, m) and wind (coloured vectors, m/s km/h) at 18:00 UTC, 25-08-2012. 00:00 UTC, 26-08-2012. The map is derived from the GFS analysis at 0.5° horizontal resolution. (For interpretation of the references to colour in this figure legend, the reader is referred to the web version of this article)

Looking at the geographic distribution and timing of lightning activity recorded by the LINET network (Betz et al., 2009), one may identify a strong convective signal elongated in southwest/northeast direction from

355

356 169

357 170

358 171

359 171

360

361

362

363

364

365

366

367

368

369

370

371

372

373

374

375

376

377

378

379

380

381 172

382 173

383 174

384 175

385 176

386 177

387 178

388 179

389 180

390 181

391

392 182

393 183

394

395 184

396 185

397

398 186

399 187

400

401 188

402

403 189

404 190

405

406 191

407 192

408

409 193

410 194

411

412

413

the central part of Piedmont region toward the Lake Maggiore area, where the lightning activity density reached its maximum, and farther northeastward (Figure 5).

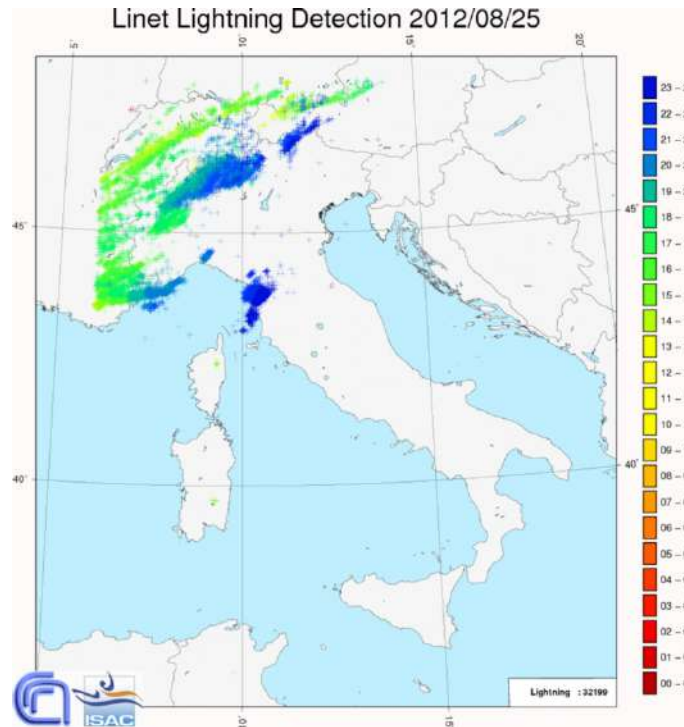


Fig. 5. Lightning activity (cloud-to-ground and intra-cloud) on 25-08-2012. The colours are representative of the different hours (UTC) of the day (courtesy of Satellite Meteorological Group of CNR-ISAC in Rome). (For interpretation of the references to colour in this figure legend, the reader is referred to the web version of this article)

3. Surface observations and radiosounding

The intensive wind-induced damages confined in a limited area suggest that the event was characterized by high wind speeds associated to a localised convective event; however, it remained unclear whether it was a tornado or a downburst. The inspection of most trees uprooted during the event and the prevailing direction along which they were inclined, from southwest to northeast, i.e. along the large-scale wind direction, suggest that the system was linear. Also, some employees of the Lake Maggiore navigation company confirmed the presence of a frontal line propagating along the lake, accompanied by rain and wind gusts (personal communication). However, a damage survey performed by one author of the present paper revealed that in some areas of Pallanza the damages were more scattered (see also Figure 1d) and the trees were inclined in different directions, thus suggesting the possible presence of a tornado, probably coexisting with the downburst. Further discussion on this point will be provided with the support of radar data in Section 6.

The data from the surface station meso-network of the Piedmont region and the meteorological radar system, consisting of two polarimetric radars and a mobile X-band radar, which is part of the national surveillance network, are considered for precipitation. Very intense rainfall concentrated for a few hours in

414
415 195 a very narrow band, extending over the Alpine foothills from Biella to Lake Maggiore and Ticino areas
416
417 196 (Figure 1); the highest rainfall amount occurred in the provinces of Verbania and Biella with a maximum of
418 197 about 93 mm in 3 hours and widespread hail (up to 6 cm, as discussed in Section 7) in these two areas
419
420 198 (ARPA Piemonte, 2012). According to a detailed analysis of the storm cells detected by the radar system
421 199 (see Section 5), the hail formed at a high altitude, due to the elevated height of the 0°C isotherm, and
422
423 200 reached the ground partially fused and mixed with rain.

424
425 201 The anemometer in Verbania Pallanza, located at the headquarters of ISE-CNR (Institute for the Study of
426 202 Ecosystems - National Research Council), in front of the Borromeo Gulf (Figure 1c), recorded the maximum
427
428 203 wind gust during the event, of about 30 m/s (about 108 km/h) at 17:58 UTC (Figure 6). The damages in the
429 204 immediate surroundings of the station were relatively minor and consistent with this measure (e.g., the
430
431 205 storm caused the breakup of some windows in the institute and the removal of few roof tails in some
432 206 houses in the surroundings). However, the damage survey suggested that the most intense part of the
433
434 207 thunderstorm struck 1 km farther away, in the gardens of Villa Taranto (Figure 1c), where hundreds of large
435 208 trees were snapped and uprooted (damage indicator 27, degree of damage 3 and 4; McDonalds and Mehta,
436
437 209 2006), suggesting that a realistic estimation of the maximum wind gust should be of about 170-220 km/h
438
439 210 (between the upper Enhanced Fujita scale EF1 rating and EF2).

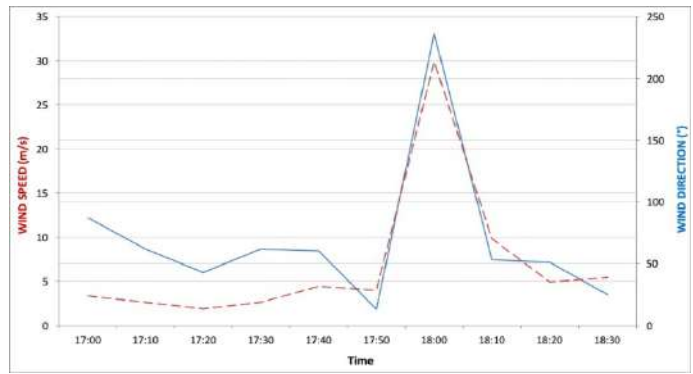
440 211 Figure 6 shows that, in correspondence with the peak in wind speed, a discontinuity was present in the
441
442 212 wind direction, as the winds rotated from northeasterly to southwesterly and, then, back to northeasterly.
443 213 The 2h-cumulated precipitation from 17:30 UTC to 19:30 UTC was about 77 mm, but a notable peak of 11.2
444
445 214 mm was measured in 2 minutes immediately after the wind gust (Figure 7). The descent of the cooler upper
446 215 level air in the downdraft and the evaporation of precipitation were responsible for a 2 m temperature
447
448 216 drop of about 12°C in 3.5 hours (5.5°C from 17:30 to 18:30 UTC).

449 217 A pre-convective proximity thermodynamic sounding in Cuneo-Levaldigi at 10:00 UTC, 25 August 2012 is
450
451 218 shown in Figure 8 (source: Department of Atmospheric Science, University of Wyoming). The sounding is
452 219 located upwind of the event, thus it may represent the characteristics of the environment before the
453
454 220 occurrence of the storm (the sounding of Milano-Linate is located downstream of the storm, thus it is not
455
456 221 representative of the environment preceding the event). The profile contains a very warm and moist
457 222 boundary layer up to about 850 hPa, above which a thermal inversion delimits a shallow layer of warm and
458
459 223 dry air; in the mid-levels, steep lapse rates are present in a deep layer. Such profiles are prototypical of the
460 224 so-called "loaded gun" sounding configuration (Wallace and Hobbs, 2006), a characteristic of an unstable
461
462 225 but capped air mass. In the sounding of Figure 8, the surface-based CAPE (Convective Available Potential
463 226 Energy) of the most unstable parcel is high (1984 J/kg) and a mechanical forcing of a few hundred meters
464
465 227 should be able to overcome the convective inhibition and to release the layer instability.

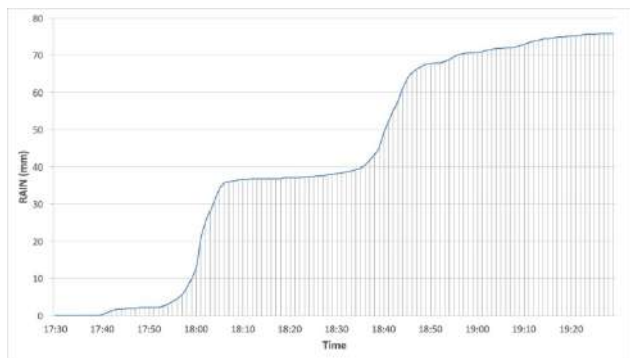
466 228 We speculate that this was indeed the case: Lake Maggiore near Verbania is located just downstream of
467
468 229 Mottarone mountain (1500 m high) with respect to the synoptic southwesterly flow. While the orography
469
470 230 triggered convection, the evaporation from the lake locally enhanced the low-level humidity compared to
471
472

473
474
475
476
477
478
479
480
481
482
483
484
485
486
487
488
489
490
491
492
493
494
495
496
497
498
499
500
501
502
503
504
505
506
507
508
509
510
511
512
513
514
515
516
517
518
519
520
521
522
523
524
525
526
527
528
529
530
531

231 that of the sounding in Figure 8, which is representative of inland, drier conditions. This effect is
232 emphasized in the Borromeo Gulf, where the orography surrounds three quarters of the water body and
233 favours the persistence of warmer and more humid air (in Verbania Pallanza, the observed relative
234 humidity at 17:30 UTC was 87%). As a consequence, near the lake the low-level dewpoint temperature
235 profile would shift to the right compared to Fig. 8, hence increasing CAPE and reducing convection
236 inhibition (CIN). The presence of more favourable low-level environmental conditions near the lake and the
237 arrival of cooler air at 850 hPa contributed to the removal of the inversion in the Verbania area, thus
238 allowing an explosive triggering of convection. Furthermore, the presence of intense vertical wind shear,
239 both in the lowest 3 km and in the 0-6 km layer (from the sounding derived by the Department of
240 Atmospheric Science, University of Wyoming, it follows that the 0-3 km (0-6 km) wind shear is about 17 m/s
241 (33 m/s)), favoured the development of a supercell.



242
243
244
245 **Fig. 6.** 10 m wind speed (red dotted line, m/s) and direction (blue solid line, deg) recorded in Verbania from 17:00 UTC
246 to 18:30 UTC. Data are instantaneous and reported every 10 minutes; the maximum wind registered at 17:58 UTC is
247 included instead of the data at 18:00 (8.1 m/s).



250
251
252 **Fig. 7.** Cumulated rainfall (mm) recorded in Verbania from 17:30 UTC to 19:30 UTC. Data are registered every minute.

532
533
534
535
536
537
538
539
540
541
542
543
544
545
546
547
548
549
550
551
552
553
554
555
556
557
558
559
560
561
562
563
564
565
566
567
568
569
570
571
572
573
574
575
576
577
578
579
580
581
582
583
584
585
586
587
588
589
590

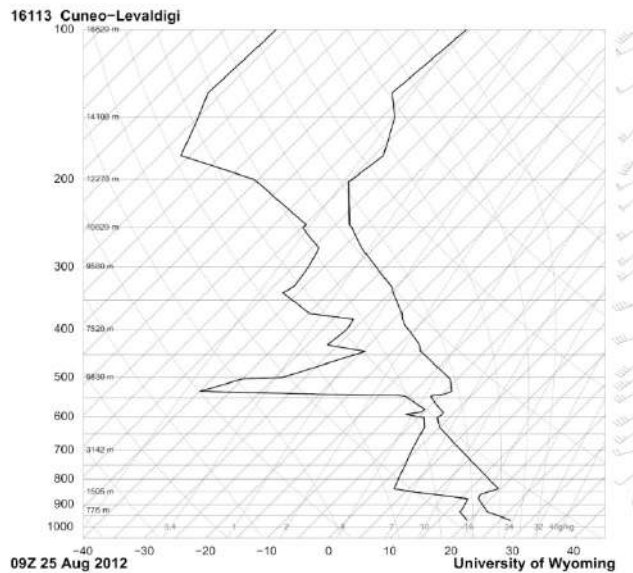


Fig. 8. Skew-T diagram in Cuneo-Levaldigi on 25 August 2012, 10:00 UTC (Source: Department of Atmospheric Science, University of Wyoming).

4. Satellite perspective

The sequence of colour-enhanced IR10.8 band satellite images from Meteosat-8 Rapid Scan Mode (Figure 9) shows that the storm responsible for the damages in Verbania had very cold (215 K) cloud top temperatures (CTTs). An explosive convective process caused a rapid decrease of CTT between 17:35 UTC and 18:15 UTC. In particular, between 17:50 and 18:10 UTC, an extended portion of the cloud top showed a remarkable temperature decrease from 215 K to 202 K. After this rapid cooling, the storm showed a cold-U shaped signature (18:20 UTC), which then developed into a cold-ring shaped signature (18:25 - 18:30 UTC). These patterns indicate that severe convective processes are taking place (Brunner et al., 2007). The very low values of CTT are indicative of a very intense updraft, which determined a significant penetration of the upper part of the storm top into the warmer lower stratosphere (Setvák et al., 2010). Although not visible in the image, the data show that the coldest temperatures of the U- and V-shaped signatures are located slightly upwind (in this case on the southwestern side) of the overshooting top (OT), while the related cold protuberances extend downwind of the OT, along the perimeter of the cirrus anvil. Usually, storms showing these signatures are present within some specific air mass types, with a relatively weak upper-level wind shear and a strong thermal inversion above the tropopause (Setvák et al., 2010). These signatures are usually short-lived, because they are dependent on the duration of the **OT cold-overshooting-top (OT)** of the cloud: the warm spot, which is located downwind, disappears when the OT decays. By analysing the images sequence, cold U-shaped or cold-rings signatures persisted between 17:35 and 18:30 UTC, confirming that the environment was very favourable to the development of severe convection.

591
592
593
594
595
596
597
598
599
600
601
602
603
604
605
606
607
608
609
610
611
612
613
614
615
616
617
618
619
620
621
622
623
624
625
626
627
628
629
630
631
632
633
634
635
636
637
638
639
640
641
642
643
644
645
646
647
648
649

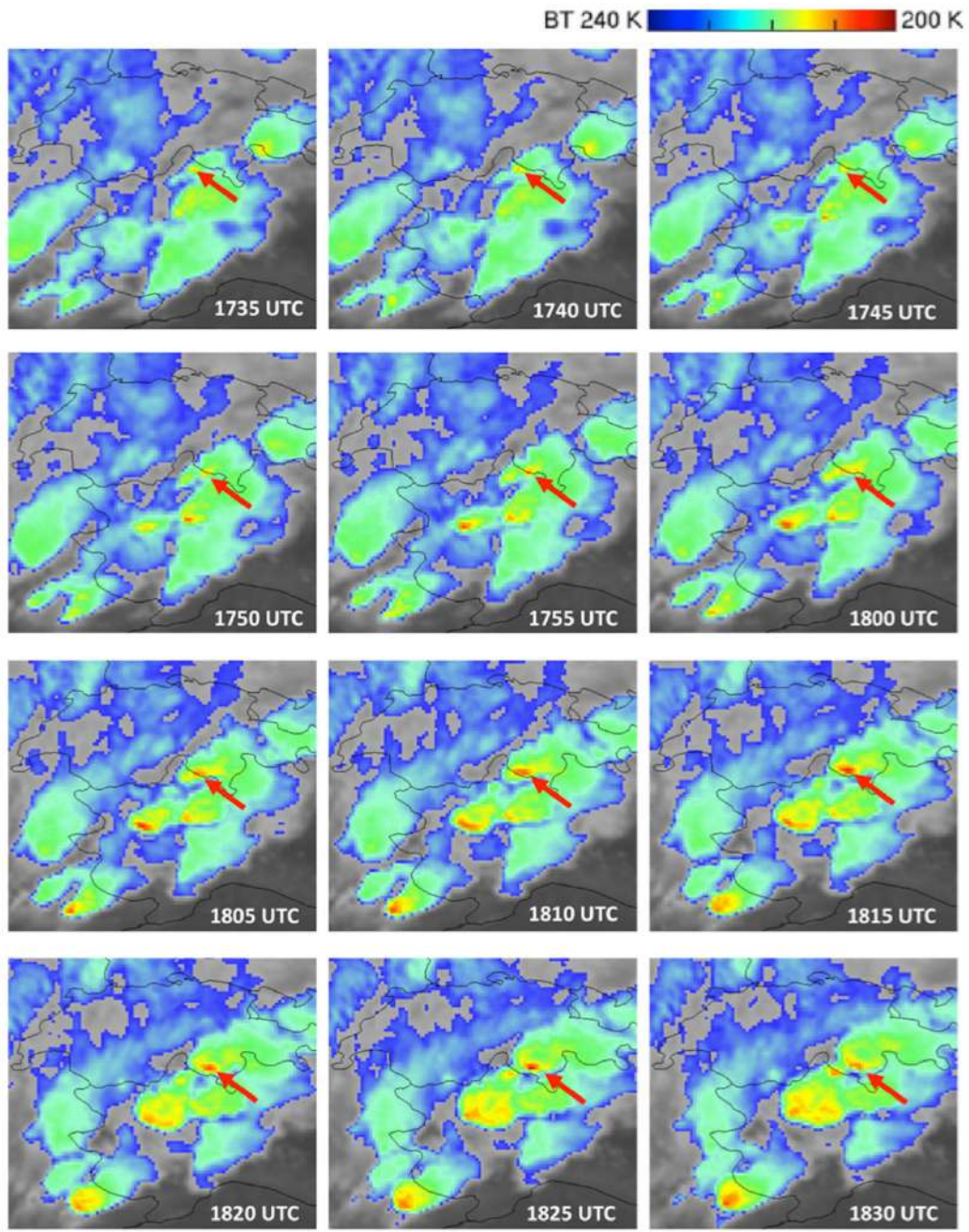


Fig. 9. Storm evolution over the Alpine region on 25 August 2012, 17:35-18:30 UTC. The Meteosat-8 colour-enhanced IR10.8 band shows a synchronized development of three severe storms. The uppermost storm, highlighted with the red arrow, is analysed in this manuscript (images are not parallax-corrected). (For interpretation of the references to colour in this figure legend, the reader is referred to the web version of this article).

5. Doppler analysis, radar tracking and hail

The radar analysis of the storm is performed using reflectivity and Doppler velocity images of the C-band radar operated by MeteoSwiss, located just 30 km northeast of the city of Verbania on the top of Monte Lema (Figure 1c), at 1600 m asl. The Swiss radar network is composed of five polarimetric C-band Doppler

650

651 radars (Germann et al., 2015). The operational scan strategy of the Swiss radars consists of 20 elevation
652
653 between -0.2° and 40° repeated every 5 min.

654 Figure 10 shows the time sequence of reflectivity and Doppler velocity measured by the Monte Lema radar
655
656 from 17:50 to 18:10 UTC, when the thunderstorm approached the Lake Maggiore and crossed the
657 Borromeo Gulf near Verbania. Between the radar site and the location of the thunderstorm there are no
658
659 mountains that may corrupt the data. Since the elevation of the radar beam is 2.5° , these images represent
660 the storm at altitudes between 3 km asl (at 17:50 UTC) and 2.5 km asl (at 18:10 UTC). Even though there
661
662 are some missing gates in the radar data, the reflectivity fields show the development of an intense
663
664 thunderstorm with a hook-echo feature at 18:05 UTC. The reflectivity values are not extreme; however,
665 they are larger than 43 dBZ, with peak values of about 50 - 55 dBZ at an elevation higher than 2.5° .

666
667 The radial Doppler velocity field clearly shows an area of outbound flow within the larger mesoscale
668
669 inbound wind, which indicates the presence of rotation associated with a mesocyclone. The gradual
670 transition between the greenish and yellow colours in the area of rotation demonstrates that the algorithm
671
672 used for the dealiasing of the radial wind field (James et al., 2001) produced a realistic field even in the
673 presence of the strong directional gradients associated with the thunderstorm. The area of rotation is
674
675 apparent in multiple volume scans and extends from about 1.5 km - the lowest height visible with the radar
676
677 - to about 4 km (not shown), thus enhancing the confidence that this feature is representative of a
678 mesocyclone.

679

680

681

682

683

684

685

686

687

688

689

690

691

692

693

694

695

696

697

698

699

700

701

702

703

704

705

706

707

708

709
710
711
712
713
714
715
716
717
718
719
720
721
722
723
724
725
726
727
728
729
730
731
732
733
734
735
736
737
738
739
740
741
742
743
744
745
746
747
748
749
750
751
752
753
754
755
756
757
758
759
760
761
762
763
764
765
766
767

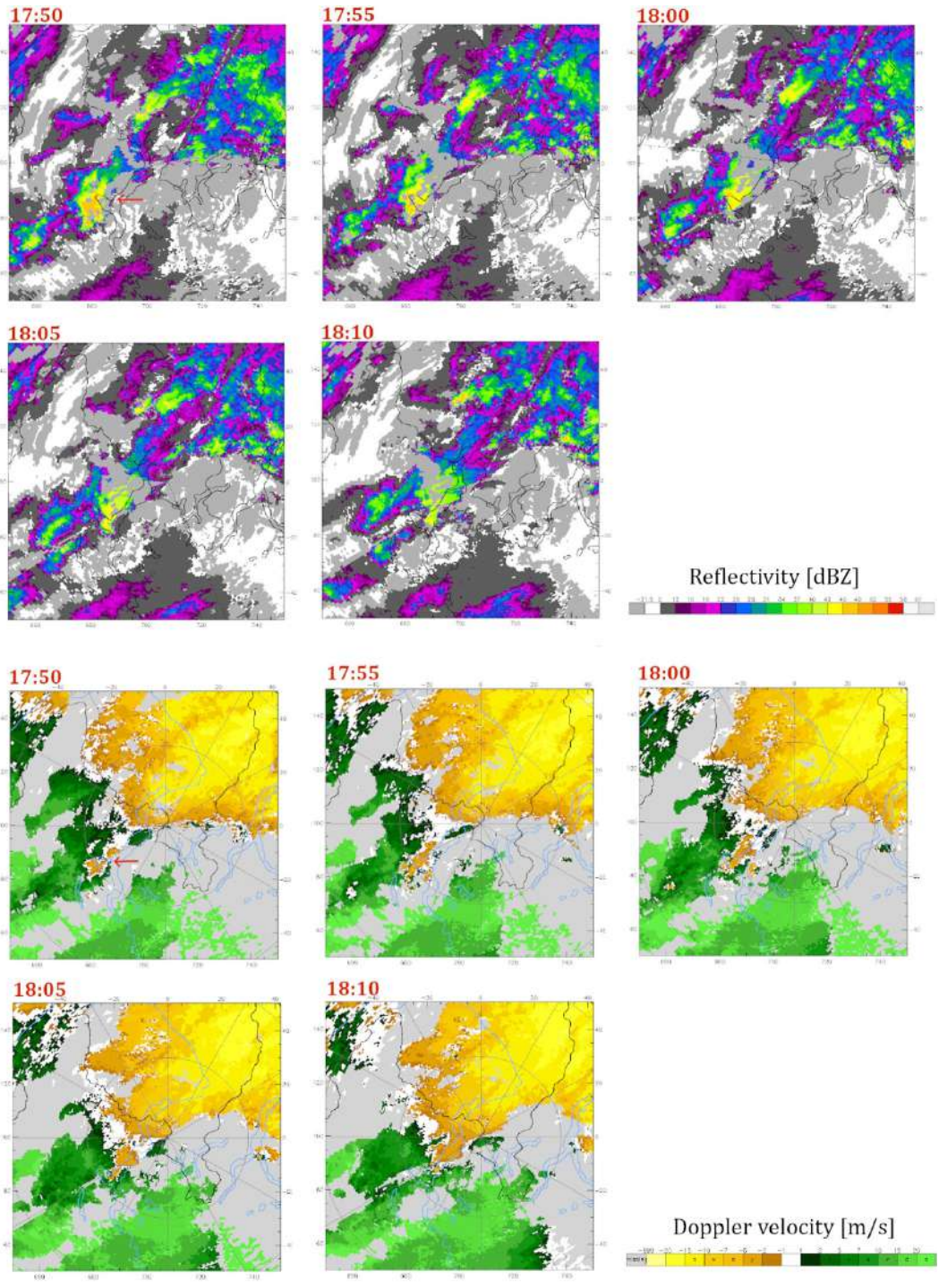


Fig. 10. Time sequence (17:50 – 18:10 UTC, 25 August 2012) of reflectivity (top, dBZ) and radial Doppler velocity (bottom, m/s), measured by the Monte Lema weather radar, at 2.5° elevation angle. The red arrows in the two 17:50 - panels indicate Verbania. The rings indicate the distances of 30 km and 60 km from the radar site. Positive values of Doppler velocity denote a wind that moves toward the radar, while negative values indicate a wind moving away from the radar. (For interpretation of the references to colour in this figure legend, the reader is referred to the web version of this article).

Although the radar in Bric della Croce (Piedmont region) was too far southwest with respect to Verbania for a detailed analysis of the storm, we show the Doppler velocity map at 18:00 UTC, 25 August 2012, to support our hypothesis of the presence of a mesocyclone. Figure 11 shows an area of inbound flow near

768
769 328 the region with the maximum reflectivity, suggesting a probable mesocyclonic rotation above the eastern
770
771 329 side of Lake Maggiore.
772

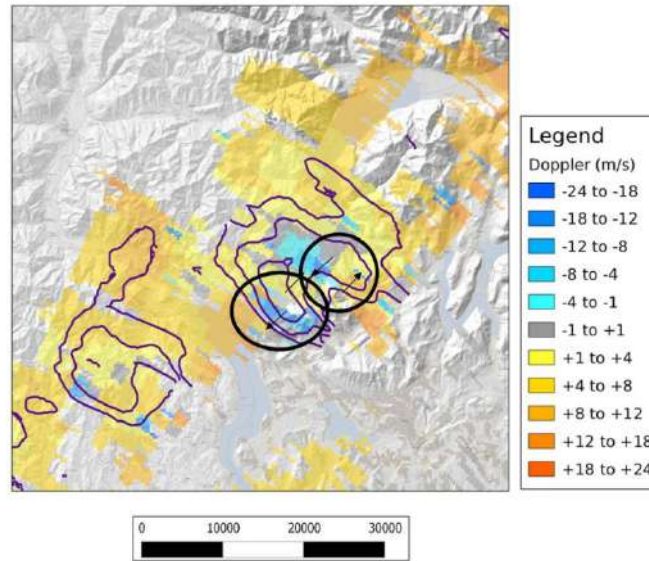


Fig. 11. Doppler velocity (m/s) measured by the “Bric della Croce” radar operated by ARPA Piedmont, on 25 August 2012, 18:00 UTC, at 0.5° elevation angle. The radar is located about 119 km southwest to Verbania (outside the domain shown in the Figure). Positive values of Doppler velocity denote a wind that moves away from the radar, while negative values indicate a wind toward the radar. The regions of probable mesocyclonic rotation are circled (black circles). The contour lines of reflectivity, with values higher than 56 dBZ, are also superposed on the map. (For interpretation of the references to colour in this figure legend, the reader is referred to the web version of this article).

803 342 The storm has also been analysed with the Thunderstorm Radar Tracking algorithm (TRT hereafter), a
804 three-dimensional multiple-radar tracking used operationally at MeteoSwiss for thunderstorms nowcasting
805 343 and storm climatological analysis (Hering et al. 2008). TRT is a two-step algorithm: the first part provides 2D
806 344 storm-objects and related geographical and geometric information (“tracking”). The second part estimates
807 the severity of the detected storms by including 3D radar data (“ranking”). The TRT output from the first
808 345 step is used here to reprocess radar data and combine the track information with hail information provided
809 346 by radar-based hail products (Nisi et al., 2018).

812 348 The storm initiated about 30 km southwest of Verbania at about 16:30 UTC (Figure 12). Within moderate
813 southwesterly steering winds, the storm reached the Verbania area in approximately one hour. Initially, the
814 349 storm was rather weak and the probability of hail was low. By the time the storm approached the Lake
815 Maggiore, the hail signal intensified considerably and reached POH (probability of hail) values greater than
816 350 70% over a large area as the storm moved northeastward. The intensification of storms near large lakes is a
817 351 common occurrence in the southern Prealpine region (MeteoSwiss forecasters, personal communication):
818 because of very moist low levels, the storm ingests a large amount of humid air in the updraft, which in
819 352 turn can enhance the latent heat release, hence the updraft intensity.
820 353
821
822 354
823 355

827

828 356 The fact that the probability of hail was high over a large area near Verbania indicates that at that time the
829
830 357 updraft of the storm was well organized and strong enough to sustain a hail core. Stronger and persistent
831 358 updrafts allow the creation of hail cores and hail stone growth in the wet and dry accretion zones in storms.
832
833 359 This process is especially efficient in the presence of large amounts of supercooled droplets, which are a
834 360 consequence of intense updrafts ingesting large amounts of humidity and increasing the buoyancy because
835
836 361 of the large latent heat release (due to condensation and glaciation processes). The more persistent the
837
838 362 hail core is, the greater the possibility for hailstones to increase in size. The estimation of hail sizes,
839 363 provided by the MESH algorithm (Maximum Estimated Severe Hail Size, not shown here; Nisi et al., 2018)
840
841 364 shows that over Verbania hail stones were rather small (< 2 cm). Larger hail sizes were apparent only at
842 365 later stages, 20-30 minutes after the storm passed over Verbania. This most likely indicates that, at the
843
844 366 time of the passage near Verbania, the hail core in the storm was rather young and the intensification of
845 367 the updraft was probably quite recent and ongoing. The results of the algorithm are consistent with ESWD
846
847 368 reports, which identify large hailstones only along the east coast of the Lake Maggiore and farther
848 369 eastward.
849

850 370

851 371

852 372

853 373

854 374

855 375

856 376

857

858

859

860

861

862

863

864

865

866

867

868

869

870

871

872

873

874

875

876

877

878

879

880

881

882

883

884

885

886
887
888
889
890
891
892
893
894
895
896
897
898
899
900
901
902
903
904
905
906
907
908
909
910
911
912
913
914
915
916
917
918
919
920
921
922
923
924
925
926
927
928
929
930
931
932
933
934
935
936
937
938
939
940
941
942
943
944

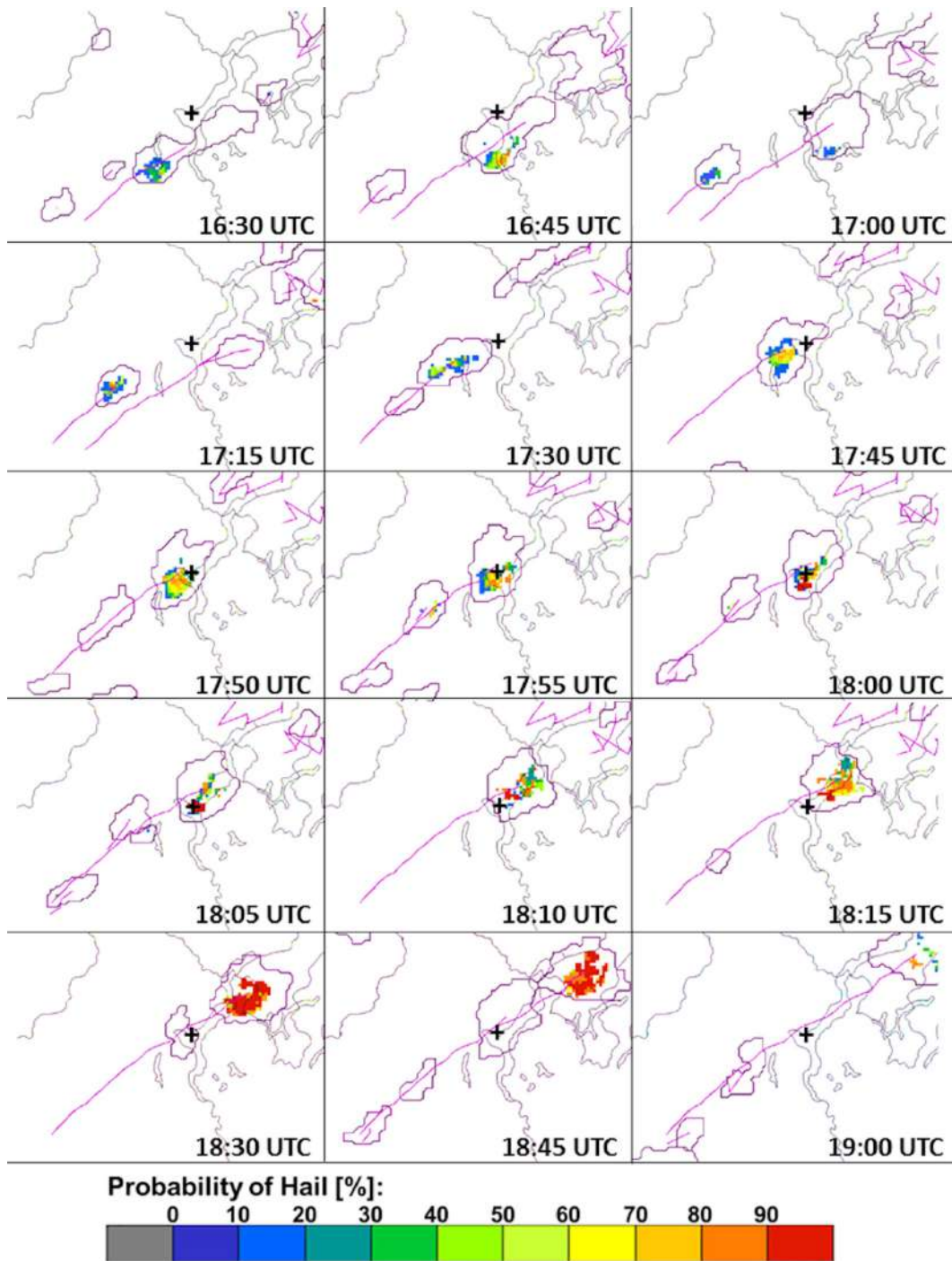


Fig. 12. Storm tracking (16:30-19:00 UTC) with the Thunderstorm Radar Tracking algorithm (Hering et al., 2008) and hail detection. The cell analysed in this study initiated in the area located west-southwest of Lake Maggiore. Colours inside the storms show the probability of hail (POH) (%). The Figure shows a rapid increase in the hail activity in the close proximity of Verbania (black 'plus sign' on the maps). (For interpretation of the references to colour in this figure legend, the reader is referred to the web version of this article).

6. Mesoscale model analysis

The fully compressible, non-hydrostatic WRF-ARW (Advanced Research WRF) model (Skamarock et al., 2008) version 3.9.1 is used here for the numerical simulation of this case study, in order to identify the atmospheric conditions responsible for severe convection and for the development of the supercell.

945
946391
947392
948393
949394
950
951395
952396
953
954397
955
956398
957399
958
959400
960401
961
962402
963403
964
965404
966405
967
968406
969
970407
971408
972
973409
974410
975
976411
977412
978
979413
980414
981
982415
983416
984417
985418
986
987419
988
989420
990
991
992
993
994
995
996
997
998
999
1000
1001
1002
1003

Set-up

Two two-way nested domains are used for the simulation (Figure 1a); the parent domain covers the central Mediterranean and the Italian peninsula (9 km grid spacing in both N-S and W-E directions; 192 x 184 grid points), while the second grid is centered over northwestern Italy (3 km grid spacing; 181x178 grid points). An additional WRF model simulation has been undertaken including a third domain, with grid spacing of 1 km, centered in the Lake Maggiore area and nested into the inner domain in Fig. 1a. However, results did not change significantly compared to those in the second grid (shown here), and are not discussed in the present study.

The model is implemented with 40 terrain-following vertical levels more closely spaced in the boundary layer, fifteen of them below 2000 m height. The simulation starts at 12:00 UTC, 24 August, and lasts 36 hours; outputs are saved every half an hour. Initial and boundary conditions are derived from the National Center for Environmental Prediction - Global Forecast System (NCEP-GFS), from the analysis cycle issued at 12:00 UTC, 24 August (0.5° horizontal resolution, fields every 3 hours).

The model configuration follows that used in Avolio et al. (2017), about the sensitivity of boundary layer variables to different parameterization schemes, and in Avolio and Federico (2018), relative to the simulation of an extreme convective event in the Mediterranean. Thus, the physical parameterizations are: the new Rapid Radiative Transfer Model (RRTMG) long-wave and short-wave radiation scheme (Iacono et al., 2008), the Noah land-surface model (Tewari et al., 2004), the Thompson microphysics scheme (Thompson et al. 2008), the Asymmetrical Convective Model version 2 (ACM2) scheme (Pleim, 2007) for the PBL, and the Betts–Miller–Janjić (BMJ) scheme cumulus parameterization (Betts and Miller, 1986). The latter is activated only for the coarse grid, while convection is explicitly resolved for the fine grid.

Precipitation patterns

Figures 13 and 14 show respectively the maximum reflectivity (observed at 18:45 UTC in radar images and simulated at 18:30 in the WRF run, inner grid) and the six-hour accumulated precipitation (simulated and observed) during the heavy rain event.

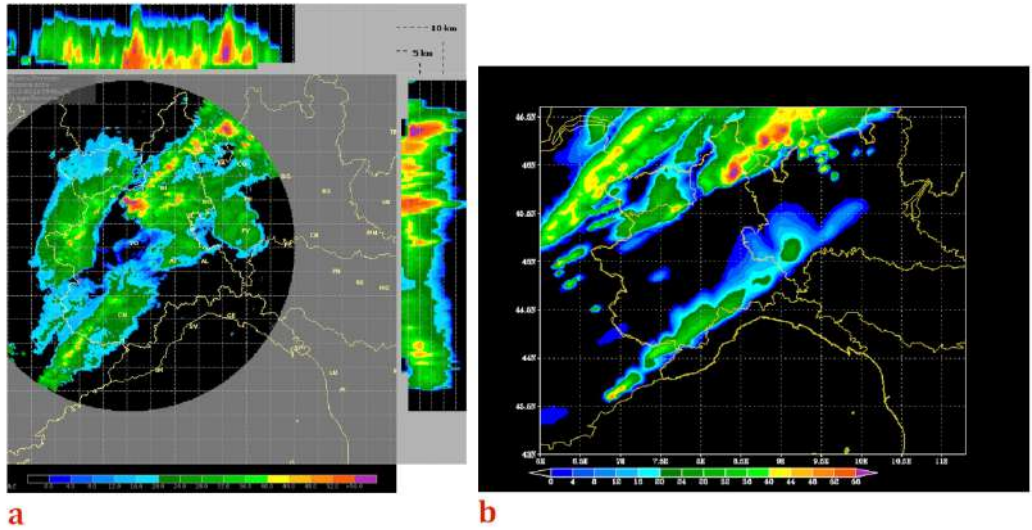


Fig. 13. left: radar reflectivity (at 18:45 UTC, 25 August; data from the Piedmont mosaic, dBZ); right: 3 km grid maximum reflectivity (dBZ) simulated by the WRF model (at 18:30 UTC, 25 August). (For interpretation of the references to colour in this figure legend, the reader is referred to the web version of this article)

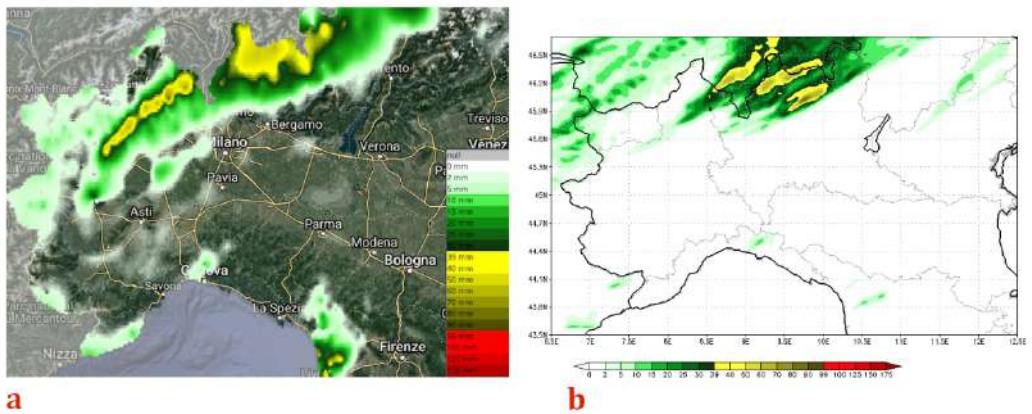


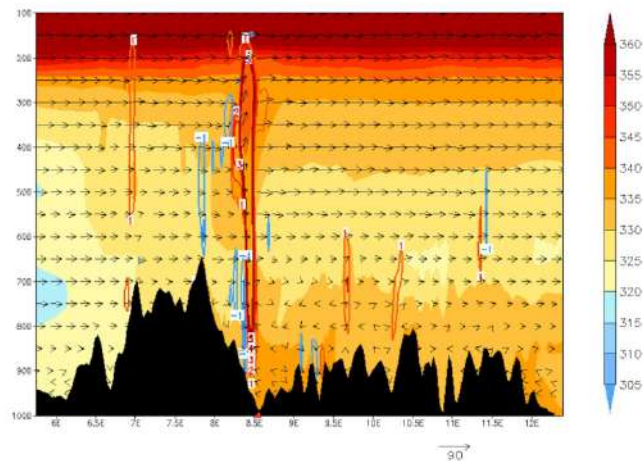
Fig. 14. left: 6h cumulated rain (mm/6h) recorded by automatic stations (data from the automatic system “Dewetra” of the Italian Department of Civil Protection; www.mydewetra.org); right: 6h cumulated rain (mm/6h) simulated by the WRF model (3 km grid spacing). Both fields are shown at 00:00 UTC, 26 August. The black dot denotes the position of Verbania. (For interpretation of the references to colour in this figure legend, the reader is referred to the web version of this article)

Figure 13 shows a good qualitative agreement. In particular, the band of high reflectivity covering the northern parts of Piedmont, with a local maximum over Ticino, and that extending on the northern side of Liguria are well reproduced (although the simulated field is slightly more extended towards the northeast). In Figure 14a, the 6-hour accumulated precipitation field, from 18:00 to 24:00 UTC on 25 August, is derived by the automatic system “Dewetra” (www.mydewetra.org), an integrated system of the Central Functional Center of the Italian Department of Civil Protection (DPC), through the interpolation of the rain gauge measurements of the national automatic stations. Apparently, the model underestimates the intensity of the rainfall (Figure 14b; the 3 km grid field is shown) in its western side, while the agreement is better in

1063
1064 445 the Lake Maggiore area, where a rain band oriented in the SW-NE direction and the areas of no rain on its
1065 south and NW side are well reproduced. In general, the whole simulated precipitation pattern, whose
1066 446 shape and maximum intensity are well reproduced, appears slightly shifted to northeast with respect to the
1067 447 observations.
1068
1069 448

1070 449 **Concerning available surface observations (Verbania Pallanza and Mottarone meteorological stations),**
1071 although a punctual comparison analysis is out of the scope of this work, we can see that the cumulated
1072 450 rain was generally underestimated by the model; e.g., in Verbania WRF simulated a daily precipitation of 31
1073 451 mm (vs. 94 mm observed) and in Mottarone 28 mm (vs. 52 mm observed). Concerning the surface
1074 452 temperature, min/max values of 18.2/28.9 °C (17.6/29.7 °C) were simulated (observed) in Verbania. Finally,
1075 453 the observed wind gust, being associated with a local event (time evolution of a few minutes), was not
1076 reproduced by the model.
1077 454

1078 455
1079 456 The vertical cross sections of equivalent potential temperature and of the vertical wind component are
1080 shown at Verbania latitude, 45.92°N in Fig. 15 (along the black line drawn in Figure 16). The frontal system
1081 457 approaches from the west: the intrusion of cooler air in mid-troposphere is visible on the left side of the
1082 Figure. Near Verbania (8.55°E), intense updrafts (flanked closely by downward motion) are apparent at
1083 458 18:30 UTC (thus, slightly later compared to the observations). Hence, the model seems able to reproduce
1084 459 the vigorous convective activity in the study area nearly at the right time. In the following subsection, we
1085 will analyse the conditions responsible for such an intense vertical motion.
1086 460
1087 461
1088 462
1089 463
1090 464
1091
1092
1093
1094
1095
1096
1097
1098
1099
1100
1101
1102
1103
1104
1105
1106
1107
1108



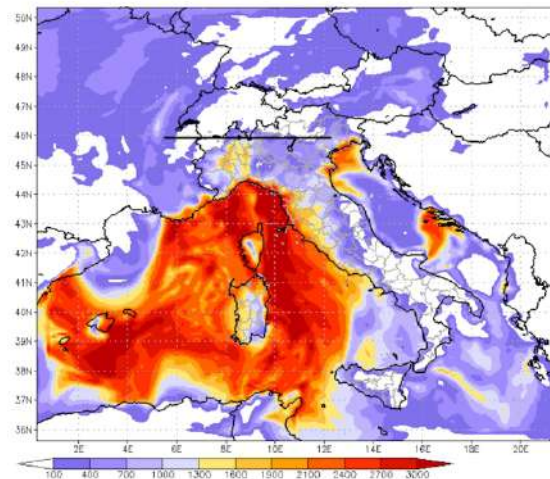
1109 465
1110 466 **Fig. 15.** WRF vertical cross section: equivalent potential temperature (shaded, K), vertical wind component (red
1111 467 contours for positive values, blue for negative; m/s), wind vector in the x-z plane at 18:30 UTC, 25 August. On the x-
1112 468 axis there are the longitudes (deg) and on the y-axis the pressure levels (mbar); the red triangle on the x-axis refers to
1113 469 the longitude of Verbania. (For interpretation of the references to colour in this figure legend, the reader is referred to
1114 470 the web version of this article)

1117 473 *Instability parameters*

1118 474
1119
1120
1121

1122
1123
1124
1125
1126
1127
1128
1129
1130
1131
1132
1133
1134
1135
1136
1137
1138
1139
1140
1141
1142
1143
1144
1145
1146
1147
1148
1149
1150
1151
1152
1153
1154
1155
1156
1157
1158
1159
1160
1161
1162
1163
1164
1165
1166
1167
1168
1169
1170
1171
1172
1173
1174
1175
1176
1177
1178
1179
1180

475 Hereafter, the analysis of some instability parameters will allow to better understand the environmental
476 conditions conducive to severe convection in this case. Figure 16 shows the CAPE of the most unstable
477 parcel (MUCAPE), as evaluated in the model outer grid at 18:00 UTC. An area of very high CAPE (> 3000
478 J/kg) affects the western Mediterranean, with a peak in the Tyrrhenian and in the Ligurian Seas; from this
479 region, a tongue of warm and moist air propagates northward across the Ligurian coasts toward the
480 Piedmont inland, enhancing the potential instability in the area.



481
482
483
484
485 **Fig. 16.** WRF-outer grid most unstable CAPE (J/kg) at 18:00 UTC, 25 August. A black line is drawn to identify the cross
486 section in Figure 15. (For interpretation of the references to colour in this figure legend, the reader is referred to the
487 web version of this article)

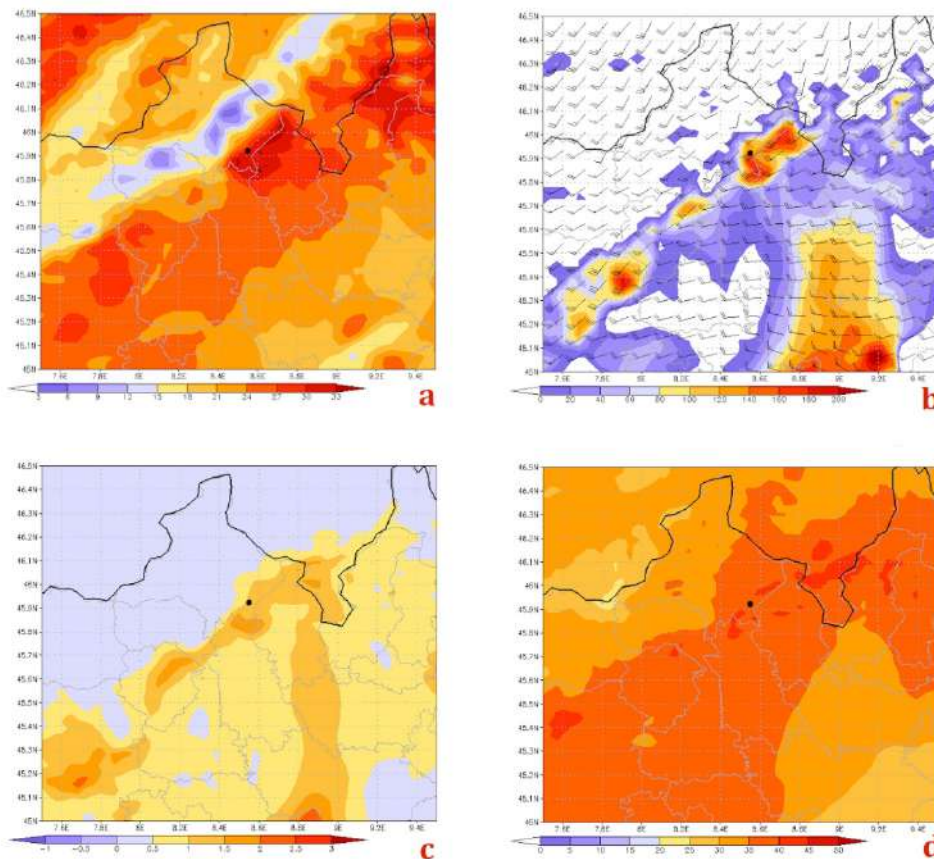


Fig. 17. WRF-inner grid (zoom): (a) 0-6 km wind difference (m/s); (b) 1km SRH (m^2/s^2); (c) EHI and (d) K-index ($^{\circ}\text{C}$). All maps refer to 18:30 UTC, 25 August. **The black dot denotes the position of Verbania.** (For interpretation of the references to colour in this figure legend, the reader is referred to the web version of this article)

Figure 17 shows the 0-6 km wind difference (a), the 0-1 km Storm Relative Helicity (SRH), (b) the Energy Helicity Index (EHI) (c), and the K-index (d). All Figures refer to the inner grid (zoomed in the area of interest) at 18:30 UTC, 25 August, i.e. the time when the model simulates the maximum convective activity in the area (similar patterns are present in the pre-convective environment 30 minutes earlier, suggesting that the high values are not affected yet by the developing convection).

In severe convective events, strong vertical wind shear enables longer storm lifetime and supports organized convective systems (e.g., supercells) that influence the severity of the storm (Markowski and Richardson, 2010). One can see, in Figure 17a, that the simulated 0-6 km wind difference in the area near Verbania was favourable to the supercell development, since it was greater than 30 m/s (a value of 15-20 m/s is generally used as discriminant; Gordon and Albert, 2000; Miller, 1972; Rasmussen and Blanchard, 1998). Similarly, the vertical wind shear was high at low levels (not shown): the simulated wind difference between 0 and 1 km exceeds 12 m/s (values greater than 5-10 m/s are considered favourable for the development of supercell and tornadoes; Craven and Brooks, 2004), and is about 22 m/s in the layer 0-3 km. This is consistent with the remark that localized severe convection episodes in Italy, tornadoes in

particular, are often associated with high values of low-level wind shear (Gaiotti et al., 2007; Miglietta and Rotunno, 2016).

As a consequence of the intense shear, the 1-km SRH, a measure of the potential for updraft rotation in supercells, reaches values up to $180 \text{ m}^2 \text{ s}^{-2}$ near Verbania (Figure 17b), i.e. above the value of $100 \text{ m}^2 \text{ s}^{-2}$ generally associated with a high threat of tornado occurrence (Davies-Jones et al., 1990). Similarly, the Energy Helicity Index $\text{EHI} = (\text{CAPE} * \text{SRH}) / (1.6 * 10^5)$, i.e. a combination of instability and wind shear, is shown in Figure 17c in the layer 0-3 km. The simulated EHI reaches a value of 2 in the area surrounding Verbania; again, this value is favourable to the development of cyclonic supercells (Davies, 1993).

Another useful diagnostic parameter related to the thunderstorm/convective potential is the K-index, based on the vertical temperature lapse rate, the moisture content of the lower troposphere, and the vertical extent of the moist layer. K is defined as: $K = (T_{850} - T_{500}) + Td_{850} - (T_{700} - Td_{700})$, where T is the temperature, Td the dew point and the subscript numbers represent the isobaric levels (hPa). Figure 17d shows that the simulated value was locally above 45°C , which denotes a high potential for convective development and thunderstorms with heavy rain (George, 1960).

Very high values are also simulated for other instability parameters (not shown), such as the Total Totals (locally greater than 55°C) and the Integrated Water Vapour (IWV; around 50 mm). In particular, the latter value is really extreme, suggesting that a huge amount of humidity was available in the vertical column to feed convection.

We summarize in Table 1 the values of the instability indices calculated in the surrounding of the Lake Maggiore, as derived from the WRF model output. The interpretation provided in Tab. 1 refers to the comparison with the climatology derived from studies mainly focused on the USA, whereas the thresholds for severe weather are generally higher than in Europe (cf. Brooks, 2009 with Romero et al., 2007). Nevertheless, the instability indices for the present case study appear relevant even in comparison with the USA climatology.

Table 1 Summary of the main instability indices simulated by WRF in the Lake Maggiore area at 18:30 UTC, 25 August 2012.

Instability Indices	WRF (simulated values in the surroundings of Verbania at 18:30 UTC, 25 August 2012)	Interpretation
MUCAPE	700-1000 J/kg	<i>moderate instability</i>
CIN	40 J/kg	<i>moderate-to-strong inhibition</i>
0-6 km Shear	30-33 m/s	<i>supercell potential</i>
0-3 km Shear	20-22 m/s	<i>supercell potential</i>
0-1 km Shear	12-13 m/s	<i>supercell potential</i>
0-3 km SRH	$> 300 \text{ m}^2/\text{s}^2$	<i>possible mesocyclone formation. Significant tornadic supercells likely</i>

0-1 km SRH	180 m ² /s ²	<i>possible mesocyclone formation. Significant tornadic supercells likely</i>
IWV	50 mm	<i>huge amount of humidity available in the vertical column (High Precipitation supercell)</i>
K-index	40-45 °C	<i>high convective potential</i>
Sweat	350-400	<i>severe thunderstorms / tornado possible</i>
T-Totals	> 55 °C	<i>severe thunderstorms likely</i>
EHI	1-2	<i>mesocyclone-induced tornadoes possible</i>

Supercell identification

The Updraft helicity (UH) is a diagnostic field introduced in Kain et al. (2008) in order to track rotation in simulated storms; it is calculated taking the integral of the vertical vorticity times the updraft velocity between 2 and 5 km AGL. Several studies have demonstrated the utility of UH in predicting tornado severity (Clark et al., 2012). In our case, this parameter is examined to identify a possible mesocyclonic circulation indicative of the presence of a supercell, as that present in the Doppler radar velocity, and to track its motion over the area of Verbania.

Figure 18 shows the UH simulated by WRF at 18:30 (fig 18a) and 19:00 (fig 18b) UTC: the sequence shows the northeastward motion of the cell crossing Verbania, with an estimated translation speed of more than 10 m/s and values of UH greater than 100 m²/s², denoting intense helicoidal ascending motion typical of a well-developed supercell. Figures 19a (18:30 UTC) and 19b (19:00 UTC) show the storm-relative velocity, obtained by subtracting the translational motion of the cell from the horizontal wind, together with the 700 hPa vertical wind component. These Figures show the presence of rotation in the cell, occurring during its translation from SW to NE, together with the presence of an updraft and a downdraft near the centre. The presence of a main updraft on the southeastern side of the storm and of large areas of downdrafts on the west and north side, are typical of mesocyclones (Klemp, 1987). The region of descending currents, consisting of dry air wrapping around the cell, is often characterized by heavy rain and hail, and has been correlated to tornado formation when concomitant with radar hook echoes (Fujita, 1975; Lemon and Doswell, 1979; Davies-Jones, 1982).

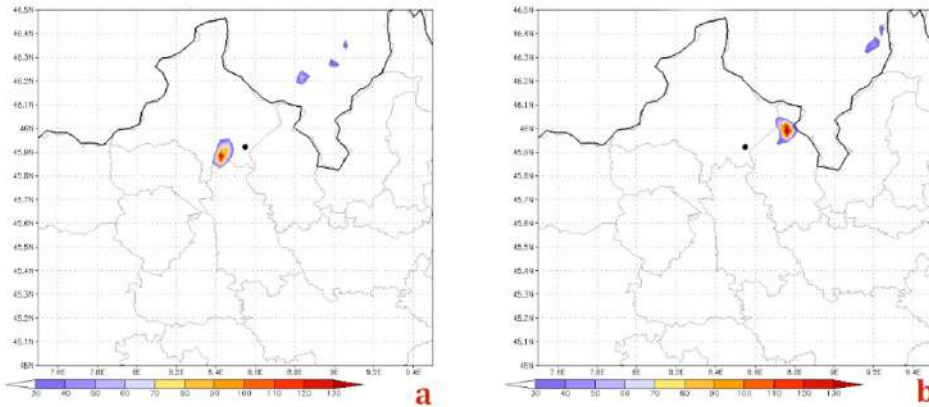


Fig. 18. WRF-inner grid (zoom) updraft helicity (shaded; values $> 30 \text{ m}^2/\text{s}^2$) at 18:30 UTC (a) and 19:00 UTC (b), 25 August. **The black dot denotes the position of Verbania.** (For interpretation of the references to colour in this figure legend, the reader is referred to the web version of this article)

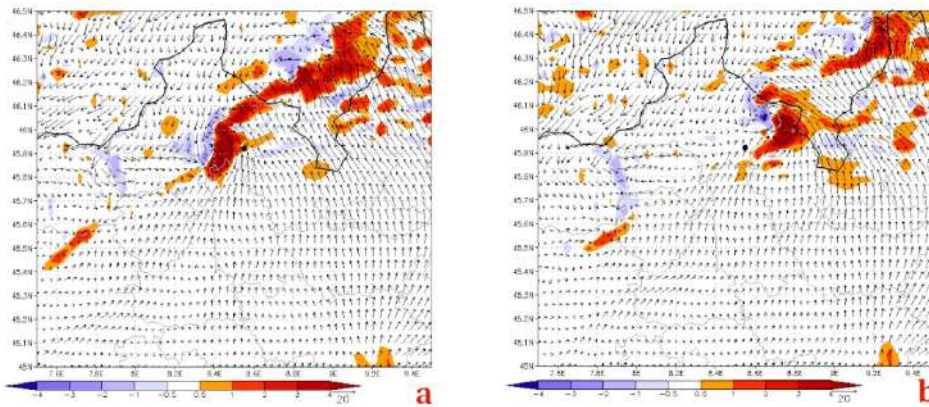


Fig. 19. WRF-inner grid (zoom) 700 hPa vertical wind speed (colours, m/s) and "storm-relative" wind (vectors), at 18:30 UTC (a) and 19:00 UTC (b), 25 August. **The black dot denotes the position of Verbania.** (For interpretation of the references to colour in this figure legend, the reader is referred to the web version of this article)

7. Conclusions

A detailed analysis of the meteorological conditions that led to a severe storm in northwestern Italy (Lake Maggiore area) on 25 August 2012, characterized by heavy rain, hail and strong wind gusts, is presented. The study was carried out through an integrated approach that involves numerical simulations, satellite and radar data, and surface/upper air measurements.

The synoptic analysis reveals that the intrusion of cooler air at mid-upper levels, the presence of a jet stream over the Lake Maggiore area, along with very hot and humid air in the PBL, helped to create conditions of high potential instability. The mechanical forcing of the nearby orography triggered convection, while the warm surface of Lake Maggiore possibly contributed to remove the thermal inversion and created a low-level environment favourable to the development of severe convection.

1417
1418
1419
1420
1421
1422
1423
1424
1425
1426
1427
1428
1429
1430
1431
1432
1433
1434
1435
1436
1437
1438
1439
1440
1441
1442
1443
1444
1445
1446
1447
1448
1449
1450
1451
1452
1453
1454
1455
1456
1457
1458
1459
1460
1461
1462
1463
1464
1465
1466
1467
1468
1469
1470
1471
1472
1473
1474
1475

589 High-resolution WRF model numerical simulations showed that the main convective features of the event were successfully reproduced. High values of several instability parameters, usually adopted in convective analysis, were simulated; the values were above the typical thresholds considered for the occurrence of severe weather.

593 The satellite analysis confirmed that severe convective processes were active, characterized by intense updrafts that penetrated into the lower stratosphere. After a rapid cloud top cooling, the storm assumed a cold-U shaped signature, which later developed into a cold-ring shape; both features are typical of severe convection and indicate the presence of an intense updraft.

597 Reflectivity and Doppler radar velocity data allowed to identify the development of an intense storm characterised by internal rotation, suggesting the presence of a mesocyclone. A specific Thunderstorm Radar Tracking algorithm reconstructed the storm motion, confirming the results emerging from the updraft helicity and storm-relative velocity simulated with the WRF model. An increase in hail activity was shown when the storm moved near Verbania, suggesting that the updraft was well organized and strong enough to sustain a hail core. The radar-based hail size estimation (MESHS) showed that hail stones were initially small (< 2 cm), while greater hail sizes (till 5 – 6 cm) were produced 20 – 30 minutes after the storm passed over Verbania. This is an indication that the storm had a strong and persistent updraft for some tens of minutes.

606 Although radar data and WRF model simulations agree in identifying a mesocyclonic circulation, **and the first damage survey suggested the possible coexistence of a tornado and a downburst**, we cannot draw definitive conclusions about the exact nature of the event. Possibly, very high-resolution numerical simulations (grid spacing of the order of 100 m) would be required to better understand the nature of the event and to determine its character, i.e. linear (downburst) or rotational (tornado).

613 Acknowledgments

614
615 LINET data were provided by Nowcast GmbH (<https://www.nowcast.de/>) within a scientific agreement between H.-D. Betz and the Satellite Meteorological Group of CNR-ISAC in Rome. The Regional Agency for the Protection of the Environment of Piedmont region (ARPA Piemonte) is acknowledged for the radar images and for surface data. Special thanks to IRSA-CNR, former ISE-CNR, for the surface data on Verbania Pallanza, and to the Italian Department of Civil Protection for the observed precipitation map (derived by the automatic system Dewetra).

623 References

624 ARPA Piemonte (The Regional Agency for the Protection of the Environment of Piedmont), 2012. Event Analysis available on line: http://www.arpa.piemonte.it/approfondimenti/temi-ambientali/meteorologia-e-clima/meteo/documenti-e-dati/evento_25_08_2012.pdf, last access 31 Dec 2019.

1476
1477 627 Avolio, E., Federico, S., Miglietta, M.M., Lo Feudo, T., Calidonna, C.R., Sempreviva, A.M., 2017. Sensitivity analysis of
1478 628 WRF model PBL schemes in simulating boundary-layer variables in southern Italy: an experimental campaign. *Atmos.*
1479 629 *Res.* 192, 58–71.
1480
1481 630 Avolio E. and Federico S., 2018. WRF simulations for a heavy rainfall event in southern Italy: Verification and sensitivity
1482 631 tests. *Atmos. Res.* 209, 14-35.
1483
1484 632 Betts, A.K., Miller, M.J., 1986. A new convective adjustment scheme. Part II: Single column tests using GATE wave,
1485 633 BOMEX, ATEX and arctic air-mass data sets. *Q. J. R. Meteorol. Soc.* 112, 693–709.
1486
1487 634 Betz, H.-D., Schmidt, K., Laroche, P., Blanchet, P., Oettinger, P., Defer, E., Dziewit, Z., and Konarski, J., 2009. LINET-an
1488 635 international lightning detection network in Europe, *Atmos. Res.*, 91, 564– 573.
1489
1490 636 Brooks, H. E., 2009. Proximity soundings for severe convection for Europe and the United States from reanalysis data.
1491 637 *Atmos. Res.*, 93, 546–553.
1492
1493 638 Brunner, J.C., Ackerman, S.A., Bachmeier, A.S., and Rabin, R.M., 2007. A quantitative analysis of the enhanced-V
1494 639 Feature in relation to severe weather. *Wea. Forecasting*, 22, pp 853-872.
1495
1496 640 Clark, A. J., J. S. Kain, P. T. Marsh, J. Correia Jr., M. Xue, and F. Kong, 2012. Forecasting tornado pathlengths using a
1497 641 three-dimensional object identification algorithm applied to convection-allowing forecasts. *Wea. Forecasting*, 27,
1498 642 1090–1113.
1499
1500 643 Craven, J.P. and Brooks, H.E., 2014. Baseline climatology of sounding derived parameters associated with deep moist
1501 644 convection. *Natl. Weather Dig.* 28, 13–24.
1502
1503 645 Davies-Jones, R. P., 1982. Observational and theoretical aspects of tornadogenesis. *Intense Atmospheric Vortices*, L.
1504 646 Bengtsson and J. Lighthill, Eds. Springer-Verlag, 175–189.
1505
1506 647 Davies-Jones, R., D. W. Burgess, and M. Foster, 1990. Test of helicity as a forecast parameter. Preprints, 16th Conf. on
1507 648 Severe Local Storms, Kananaskis Park, AB, Canada, *Amer. Meteor. Soc.*, 588–592.
1508
1509 649 Davies, J. M., 1993. Small tornadic supercells in the central plains. Preprints, 17th Conf. Severe Local Storms, St. Louis,
1510 650 MO, *Amer. Meteor. Soc.*, 305-309.
1511
1512 651 Doswell, C. A., III, G. W. Carbin, and H. E. Brooks, 2012. The tornadoes of spring 2011 in the USA: An historical
1513 652 perspective. *Weather*, 67, 88–94.
1514
1515 653 **Dotzek, N., Groenemeijer, P., Feuerstein, B., Holzer, A.M., 2009. Overview of ESSL's severe convective storms research**
1516 654 **using the European Severe Weather Database ESWD. *Atmos. Res.* 93, 575-586.**
1517
1518 655 Fujita, T. T., 1975. New evidence from the April 3–4, 1974 tornadoes. Preprints, Ninth Conf. on Severe Local Storms,
1519 656 Norman, OK, *Amer. Meteor. Soc.*, 248–255.
1520
1521 657 George, J. J., 1960. *Weather forecasting for aeronautics*, Academic press, 673 pp..
1522
1523 658 Germann, U., Boscacci, M., Gabella, M. and Sartori, M., 2015. Radar design for prediction in the Swiss Alps.
1524 659 *Meteorological Technology International*, 4, 42–45.
1525
1526 660 Gaiotti, D. B., Giovannoni, M., Pucillo, A., & Stel, F., 2007. The climatology of tornadoes and waterspouts in Italy.
1527 661 *Atmos. Res.*, 83, 534–541.
1528
1529 662 Gianfreda, F., Miglietta, M. M., Sansò, P., 2005. Tornadoes in southern Apulia (Italy). *Natural Hazards*, 34, 71–89.
1530
1531 663 Gordon, J. and Albert, D., 2000. A comprehensive severe weather fore-cast checklist and reference guide, Noaa
1532 664 technical service publication, TSp 10, NWS central region.
1533
1534

1535
1536
1537 665 Hering, A.M., Germann, U., Boscacci, M. and S n si, S., 2008. Operational nowcasting of thunderstorms in the Alps
1538 666 during MAP D-PHASE. In: Proceedings of 5th European Conference on Radar in Meteorology and Hydrology (ERAD), 30
1539 667 June–4 July 2008, Helsinki, Finland. Copernicus: G ttingen, pp. 1–5.
1540
1541 668 Homar, V., M. Gay , R. Romero, C. Ramis, and Alonso S., 2003. Tornadoes over complex terrain: An analysis of the
1542 669 28th August 1999 tornadic event in eastern Spain. *Atmos. Res.*, 67–68, 301–317.
1543
1544 670 Iacono, M.J., Delamere, J.S., Mlawer, E.J., Shephard, M.W., Clough, S.A., Collins, W.D., 2008. Radiative forcing by long-
1545 671 lived greenhouse gases: calculations with the AER radiative transfer models. *J. Geophys. Res.* 113, D13103.
1546
1547 672 Isotta, F.A., Frei, C., Weilguni, V., Tadi , M.P., Lassegues, P., Rudolf, B., Pavan, V., Cacciamani, C., Antolini, G., Ratto,
1548 673 S.M., Munari, M., Micheletti, S., Bonati, V., Lussana, C., Ronchi, C., Panettieri, E., Marigo, G. and Verta nik, G., 2014.
1549 674 The climate of daily precipitation in the Alps: development and analysis of a high-resolution grid dataset from
1550 675 pan-Alpine rain-gauge data. *International Journal of Climatology*, 34, 1657–1675.
1551
1552 676 James, N. C and R. A. Houze, 2001. A Real-Time Four-Dimensional Doppler Dealiasing Scheme. *Journal of Atmospheric*
1553 677 *and Oceanic Technology*, 18, 1674–1683.
1554
1555 678 Jans , A., Alpert, P., Arbogast, P., Buzzi, A., Ivancan-Picek, B., Kotroni, V., Llasat, M., Ramis, C., Richard, E., Romero, R.,
1556 679 et al., 2014. MEDEX: a general overview. *Nat. Haz. Earth Syst. Sci.* 14 (8), 1965–1984.
1557
1558 680 Jirak, I. L., W. R. Cotton, and R. L. McAnelly, 2003. Satellite and radar survey of mesoscale convective system
1559 681 development. *Mon. Wea. Rev.*, 131, 2428–2449.
1560
1561 682 Kain, J. S., and Coauthors, 2008. Some practical considerations regarding horizontal resolution in the first generation
1562 683 of operational convection-allowing NWP. *Wea. Forecasting*, 23, 931–952.
1563
1564 684 Klemp, J. B., 1987. Dynamics of tornadic thunderstorms. *Annu. Rev. Fluid Mech.*, 19, 369–402.
1565
1566 685 Lemon and C. A. Doswell, 1979. Severe thunderstorm evolution and mesocyclone structure as related to
1567 686 tornadogenesis. *Mon. Wea. Rev.*, 107, 1184–1197.
1568
1569 687 Lionello, P., and Coauthors, 2006. The Mediterranean climate: An overview of the main characteristics and issues.
1570 688 *Mediterranean Climate Variability*, Eds., Elsevier, 1–26.
1571
1572 689 Markowski, P. and Richardson, Y., 2010. *Mesoscale meteorology in midlatitudes*. John Wiley & Sons, 420 pp.
1573
1574 690 Matsangouras, I. T., Nastos, P. T., Bluestein, H. B., & Sioutas, M. V., 2014. A climatology of tornadic activity over
1575 691 Greece based on historical records. *International Journal of Climatology*, 34, 2538–2555.
1576
1577 692 Matsangouras, I. T., Nastos, P. T., Bluestein, H. B., Papachristopoulou, K., Pytharoulis, I., & Miglietta, M. M., 2017.
1578 693 Analysis of waterspout environmental conditions and of parent-storm behaviour based on satellite data over the
1579 694 southern Aegean Sea of Greece. *International Journal of Climatology*, 37, 1022–1039.
1580
1581 695 McDonald, J., and K. C. Mehta, 2006. A recommendation for an Enhanced Fujita Scale (EF-Scale), Revision 2. Wind
1582 696 Science and Engineering Research Center, Texas Tech University, 111 pp.
1583
1584 697 Miglietta M.M., Matsangouras I.T., 2018. An updated “climatology” of tornadoes and waterspouts in Italy. *Int J Climatol.*,
1585 698 1–17.
1586
1587 699 Miglietta, M. M., & Rotunno, R., 2016. An EF3 multivortex tornado over the Ionian region: Is it time for a dedicated
1588 700 warning system over Italy? *Bulletin of the American Meteorological Society*, 97, 337–344.
1589
1590 701 Miglietta M.M., Manzato A., and Rotunno R., 2016. Characteristics and Predictability of a Supercell during HyMeX
1591 702 SOP1. *Q. J. Roy. Meteor. Soc.*, 142, 2839–2853.
1592
1593

1594

159503 Miglietta, M.M., Mazon J., and Rotunno R., 2017a. Numerical Simulations of a Tornadic Supercell over the
159604 Mediterranean. *Wea. Forecasting*, 32, 1209–1226.

1597

159805 Miglietta M.M., Mazon J., Motola V., Pasini A., 2017b. Effect of a positive Sea Surface Temperature anomaly on a
159906 Mediterranean tornadic supercell, *Scientific Reports*, 7, 12828, 1-8.

1600

160707 Miller, R. C., 1972. Notes on analysis and severe storm forecasting procedures of the Air Force Global Weather Center,
160708 AWS Tech. Report 200 (Rev.), Headquarters Air Weather Service, Scott AFB, 106 pp..

1603

160709 Nisi, L., O. Martius, A. Hering, M. Kunz & Germann, U., 2016. Spatial and temporal distribution of hailstorms in the
160710 Alpine region: a long-term, high resolution, radar-based analysis. *Quarterly Journal of the Royal Meteorological*
160711 *Society*, 142(697), 1590-1604.

1607

160712 Nisi, L., Hering, A., Germann, U., & Martius, O., 2018. A 15-year hail streak climatology for the Alpine region. *Quarterly*
160713 *Journal of the Royal Meteorological Society*, 144(714), 1429-1449.

1610

161714 Peyraud, L., 2013. Analysis of the 18 July 2005 Tornadic Supercell over the Lake Geneva Region. *Wea. Forecasting*, 28,
161715 1524–1551.

1613

161716 Pleim, J.E., 2007. A combined local and non-local closure model for the atmospheric boundary layer. Part 1: model
161717 description and testing. *J. Appl. Meteorol. Climatol.* 46, 1383–1395.

1616

161718 Panziera, L. & Germann, U., 2010. The relation between airflow and orographic precipitation on the southern side of
161719 the Alps as revealed by weather radar. *Quarterly Journal of the Royal Meteorological Society*, 136(646), 222-238.

1619

162020 Panziera, L., James, C.N. & Germann, U., 2015. Mesoscale organization and structure of orographic precipitation
162021 producing flash floods in the Lago Maggiore region. *Quarterly Journal of the Royal Meteorological Society*, 141(686),
162022 224-248.

1623

162023 Panziera, L., Gabella, M., Germann U. & Martius, O., 2018. A 12-year radar-based climatology of daily and sub-daily
162024 extreme precipitation over the Swiss Alps. *International Journal of Climatology*, 38 (10), 3749-3769.

1625

1626

162725 Rasmussen, E.N., and D.O. Blanchard, 1998. A baseline climatology of sounding-derived supercell and tornado forecast
162726 parameters. *Wea. Forecasting*, 13, 1148-1164.

1628

1629

163027 Rodríguez, O., & Bech, J., 2018. Sounding-derived parameters associated with tornadic storms in Catalonia.
163028 *International Journal of Climatology*, 38, 2400–2414.

1631

1632

163229 Romero, R., Gaya, M. and Doswell III, C.A., 2007. European climatology of severe convective storm environmental
163230 parameters: A test for significant tornado events. *Atmos. Res.*, 83, 389-404.

1634

1635

163531 Scheffknecht, P., Serafin, S., Grubisic, V., 2017. A long-lived supercell over mountainous terrain. *Q. J. R. Meteorol.*
163532 *Soc.*, 143, 2973–2986.

1637

1638

163833 Schenkman, A.D., Xue, M., Shapiro, A., Brewster, K., Gao, J., 2011. The analysis and prediction of the 8-9 may 2007
163834 Oklahoma tornadic mesoscale convective system by assimilating WSR-88D and CASA radar data using 3DVAR. *Mon.*
164035 *Weather Rev.* 139 (1), 224–246.

1641

1642

164236 Setvák M., Lindsey D.T., Novák P., Wang P.K., Radová M., Kerkmann J., Grasso L., Su S-H., Rabin R.M., Štáštka J.,
164237 Charvát Z., Kyznarová H., 2010. Satellite-observed cold-ring-shaped features atop deep convective clouds. *Atmos. Res.*,
164238 97, 80-96.

1645

164639 Skamarock, W.C., Klemp, J.B., Dudhia, J., Gil, D.A., Barker, D.M., Duda, M.G., Huang, X.- Y., Wang, W., Powers, J.G.,
164740 2008. Description of the Advanced Research WRF Version 3. National Center for Atmospheric Research. Boulder,
164741 Colorado, USA.

1649

165042 Tewari, M., Chen, F., Wang, W., Dudhia, J., LeMone, M.A., Mitchell, K., Ek, M., Gayno, G., Wegiel, J., Cuenca, R.H.,
1651
1652

1653

1654 2004. Implementation and Verification of the Unified NOAA Land Surface Model in the WRF Model. 20th Conference
 1655 on Weather Analysis and Forecasting/16th Conference on Numerical Weather Prediction. pp. 11-15.
 1656

1657 Thompson, G., Field, P. R., Rasmussen, R. M., Hall, W. D., 2008. Explicit forecasts of winter precipitation using an
 1658 improved bulk microphysics scheme. Part II: implementation of a new snow parameterization. Mon. Weather Rev.
 1659 136, 5095-5115.
 1660

1661 Wallace, J. M., & Hobbs, P. V., 2006. Atmospheric science: an introductory survey. Amsterdam, Elsevier Academic
 1662 Press.
 1663

1664 Zanini, M. A., Hofer, L., Faleschini, F., & Pellegrino, C., 2017. Building damage assessment after the Riviera del Brenta
 1665 tornado, northeast Italy. Natural Hazards, 86, 1247-1273.
 1666

1667

1668

1669

1670

1671

1672

1673

1674

1675

1676

1677

1678

1679

1680

1681

1682

1683

1684

1685

1686

1687

1688

1689

1690

1691

1692

1693

1694

1695

1696

1697

1698

1699

1700

1701

1702

1703

1704

1705

1706

1707

1708

1709

1710

1711